

Article

Exploration on Electronic Properties of Self-Assembled Indium Nitrogen Nanosheets and Nanowires by a Density Functional Method

Running Zhao ^{1,*}, Rui Chen ¹, Hua Zhao ¹, Fan Lin ¹ and Ju-Guang Han ^{2,*} ¹ School of Arts and Sciences, Shanghai Dianji University, Shanghai 201306, China² National Synchrotron Radiation Laboratory, University of Science and Technology of China, Hefei 230029, China

* Correspondence: zhaorunning@126.com (R.Z.); jghan@ustc.edu.cn (J.-G.H.)

Abstract: Equilibrium geometries and properties of self-assembled $(\text{InN})_{12n}$ ($n = 1-9$) nanoclusters (nanowires and nanosheets) are studied using the GGA-PBE (general gradient approximation with Perdew–Burke–Ernzerh) method. The relative stabilities and growth patterns of semiconductor $(\text{InN})_{12n}$ nanoclusters are investigated. The odd-numbered nano-size $(\text{InN})_{12n}$ (n is odd) have weaker stabilities compared with the neighboring even-numbered $(\text{InN})_{12n}$ (n is even) ones. The most stable $(\text{InN})_{48}$ nanosheet is selected as a building unit for self-assembled nano-size film materials. In particular, the energy gaps of InN nanoclusters show an even–odd oscillation and reflect that $(\text{InN})_{12n}$ ($n = 1-9$) nanoclusters are good optoelectronic materials and nanodevices due to their energy gaps in the visible region. Interestingly, the calculated energy gaps for $(\text{InN})_{12n}$ nanowires varies slightly compared with that of individual $(\text{InN})_{12}$ units. Additionally, the predicted natural atomic populations of In atoms in $(\text{InN})_{12n}$ nanoclusters show that the stabilities of $(\text{InN})_{12n}$ nanoclusters is enhanced through the ionic bonding and covalent bonding of $(\text{InN})_{12n}$ ($n = 1-9$) nanoclusters.

Keywords: electronic properties; self-assembled $(\text{InN})_{12n}$ materials; growth pattern; charge transfers; nano-film



Citation: Zhao, R.; Chen, R.; Zhao, H.; Lin, F.; Han, J.-G. Exploration on Electronic Properties of Self-Assembled Indium Nitrogen Nanosheets and Nanowires by a Density Functional Method. *Molecules* **2023**, *28*, 7358. <https://doi.org/10.3390/molecules28217358>

Academic Editor: Bryan M. Wong

Received: 9 October 2023

Revised: 23 October 2023

Accepted: 28 October 2023

Published: 31 October 2023



Copyright: © 2023 by the authors. Licensee MDPI, Basel, Switzerland. This article is an open access article distributed under the terms and conditions of the Creative Commons Attribution (CC BY) license (<https://creativecommons.org/licenses/by/4.0/>).

1. Introduction

In order to develop future novel nanomaterials, the semiconducting nanostructures of materials play key roles because they uncover unique behaviors and possess widespread potential applications in energy materials and electronic and optoelectronic nanodevices [1–18]. In particular, self-assembled nanowires, which can address fundamental issues related to dimensionality, have widespread applications in optoelectronic and nano-electronic devices. The interesting properties of size-specific self-assembled nanosheets or cluster-assembled nanowires [6,8,12] allow new nanomaterials and nanodevices to be generated that can be applied to different nanoscience fields [1–3,6,8,10–21]. The individual properties of the magic stable cluster being used as a building unit for these self-assembled nanosheets, nanowires, or nanomembranes are actually maintained. It should be pointed out that cluster self-assembly is a spontaneous formation of well-defined and ordered structural forms; thus, reliable self-assembly techniques are surely suitable for different purposes for developing nanomaterials. However, these self-assembled nanostructures hold unique electronic properties and may acquire different properties or functions that differ from those observed for macroscale counterpart materials. The specific geometrical forms and electronic properties of self-assembled nanostructures have very important potential applications in energy nanomaterials and electronic nanomaterials [1,10–21]. Thus, semiconductor structured nanomaterials hold the potential to promote advancements in the rapidly growing technological fields.

It has been found that metal oxides (ZnO, Al₂O₃, and MgO), metal sulfides (Cu₃S₃, CdS, and ZnS), and transition metal nitrides (GaN, AlN, and InN), together with their

cluster-assembled nanomaterials, are of very high interest and have been widely investigated [1–5,7–17,19–21], and the possible geometries and energy gaps of inner hollow semiconductor (GaN)_{2n} nanocages have been confirmed [21]. It has been found that the stable GaN and InN nanocages are good semiconductor materials with stronger electron mobility, which is consistent with experimental values [9,11,13,14]. Moreover, the relative stabilities of nano-size (InN)_{2n} and (CdS)_{2n} (n = 5–27) clusters have been studied, and the photon-to-current conversion efficiency related to the energy conversion of inner hollowed nano-size Cd_{2n}S_{2n} (n = 5–27) clusters has been discussed [7,9]. Among these structured nanomaterials, ultrathin two-dimensional (2D) nanomaterials and quantum size effects have received attention because of their applications and new properties [12]. (GaN)_n, (AlN)_n (n = 4–6), and (InN)_n clusters, together with bulk and 2D InN crystals, have been predicted theoretically [1,8,12]. The density functional theory (DFT) method confirms that AlP material, with high photoelectron absorption, is an indirect semiconductor material, whereas GaP, GaN, and AlN are direct semiconductor nanomaterials with energy band gaps predicted to be 4.51, 2.36, 1.84, and 2.01 eV, respectively. Moreover, AlP/GaP/AlN/GaN materials demonstrate potential applications [21]. Single-crystalline AlN nanotubes and nanowires, with diameter regions from 2.2 to 0.7 nm, have been explored theoretically [12]. Consequently, significant progress has been achieved in structure determination and electronic property evaluation for nanosheets and nanowires, particularly for self-assembled (InN)_{12n} superclusters or nanomembranes. Stable (InN)_{12n} units can self-assemble 2D atomic mono-layer nanosheets, nanowires, and In₁₂N₁₂ aggregated superclusters, with important applications for microelectronic and optoelectronic nanodevices. Interestingly, InN nanosheets, with the highest electron mobility and the lowest effective electron mass, are suitable for high-frequency and high-power nanodevices [14].

The computational simulations and experimental measurements of properties for self-assembled (InN)_{12n} superclusters originating from the (InN)₁₂ units have not been fully studied due to the current experimental challenges in identifying their geometries. In order to obtain all of the possible properties and growth patterns of self-assembled (InN)_{12n} nanosheets or nanowires, to clarify the relationship between electronic structures and geometrical configurations, and to explore their important applications, a number of self-assembled (InN)_{12n} nanosheets and nanowires originating from (InN)₁₂ units were designed and predetermined with DFT methods. However, geometries and electronic structures of self-assembled (In₁₂N₁₂)_n nanoclusters linked by six-membered rings had not been carried out previously. Consequently, this computational investigation focuses on the predictions and determinations of the favorable growth patterns, stabilities, geometries, and electronic properties, as well as the driving forces, of self-assembled semiconductor (InN)_{12n} nanosheets and nanowires formed by individual (InN)₁₂ units bonded together by six-membered rings using established density functional methods.

2. Computational Details

Geometrical and electronic properties of self-assembled (InN)_{12n} nanoclusters (nanowires and nanosheets) with elemental (InN)₁₂ units were combined by means of a six-membered ring, performed by DFT (density functional theory) simulations with the gradient-corrected PBE (Perdew–Burke–Ernzerh) [22] of the exchange–correlation functional within the Kohn–Sham framework of the density functional theory, as implemented in the GAUSSIAN09 RevD.01 package [23]. The exchange and the correlation part in PBE1PBE were specified as follows: The “1” stands for “1 parameter hybrid”, i.e., the functional consists of 25% from Hartree–Fock and 75% from PBE for the exchange part, and then the correlation maintains the PBE part (it is the same as PBE0 [24]). This means that the hybrid PBE0 functional compensates for part of the inaccuracy of the PBE XC by adding a fraction of the exact exchange, allowing for more accurate results in the evaluation of the energy gap. Energy gaps are calculated with increased accuracy with this

method compared to “standard” PBE. The accurate electronic properties and geometries of self-assembled semiconductor $(\text{InN})_{12n}$ superclusters can be determined by adopting 6-31G(d) and LanL2DZ basis sets for nitrogen and indium atoms, respectively. Moreover, the PBE method is suitable for calculating the metal complexes and provides a reasonable explanation of the geometries and electronic properties.

The PBE1PBE exchange–correlation functional with 6-31G(d) and LanL2DZ basis sets for N and In atoms, respectively, is already conformed to best describing the electronic structures of InN nanomaterials [9]. Using this reliable theoretical method, the electronic and geometrical properties of inner hollowed nanoscale $(\text{InN})_{2n}$ ($n = 6\text{--}27, 45, 54$) clusters can be successfully determined [9,25]. One can surely ascertain that this method is suitable for investigating self-assembled $(\text{InN})_{12n}$ superclusters (or nanoclusters) and provides reliable geometrical forms and reasonable electronic properties. The optimized geometries of all self-assembled $(\text{InN})_{12n}$ nanoclusters were systematically determined. In addition, zero-point vibrational energy was taken into account, and the total energy of $(\text{InN})_{12n}$ was calculated. In order to test the stabilities of $(\text{InN})_{12n}$ nanoclusters (nanosheets and nanowires), their harmonic vibrational frequencies were considered and evaluated to determine the clusters’ stabilities. Zero-point vibrational energy (ZPVE) was included in the total energy and all calculations were carried out at 298.15 K under a 1 atmosphere. In addition, it is well known that the HOMO-LUMO gaps of nanoclusters can be influenced by their size; it is difficult to predict the quantum size effect by using the PBE1PBE method accurately. However, range-separated functionals can yield slight corrections of the calculated HOMO-LUMO gaps of $(\text{InN})_{12n}$ nanoclusters [26,27]. In this article, the simulations of HOMO, LUMO, and HOMO-LUMO gaps at the PBE1PBE level considering range-separated functionals is ignored due to the extensive computational time.

3. Results and Discussion

Recent experimental measurements exhibited that InN nanosheets or nanowires with the highest electron mobility and the lowest effective electron mass are widely suitable for high-power and high-frequency devices and have significant applications in optoelectronic nanodevices [1,8,28]. Consequently, studies of newly self-assembled $(\text{InN})_{12n}$ nanosheets and nanowires are opening interesting research fields for developing next-generation nanomaterials with unique properties. In order to self-assemble $(\text{InN})_{12n}$ nanoclusters with the aid of DFT methods, the selected linking or bonding atoms connecting individual $(\text{InN})_{12}$ units are very critical for forming specific nanomaterials with unique electronic properties. That is to say, the selected linking ligands or bonds between two individual $(\text{InN})_{12}$ units can lead to different geometrical structures of self-assembled $(\text{InN})_{12n}$ nanowires and nanosheets, resulting in different properties and applications. In order to form more stable self-assembled $(\text{InN})_{12n}$ nanowires and nanosheets connected by six-membered rings of individual $(\text{InN})_{12}$ units, in this study, the selected linking atoms in six-membered rings of an $(\text{InN})_{12}$ cage differed from the atom types in other six-membered rings of $(\text{InN})_{12}$ units. As far as the self-assembled $(\text{InN})_{12n}$ superclusters connected by six-membered rings are concerned, detailed studies of the self-assembled $(\text{InN})_{12n}$ nanosheets and nanowires were taken into account by using the PBE1PBE method.

3.1. Geometries and Stabilities

In order to provide an accurate understanding of the geometrical and electronic properties of $(\text{InN})_{12n}$ nanosheets with $n = 1\text{--}8$ (Figure 1 and Table 1) and $(\text{InN})_{12n}$ nanowires with $n = 1\text{--}9$ (Table 2 and Figure 2), beginning with the predictions of the accurate geometrical forms of $(\text{InN})_{12n}$ ($n = 1\text{--}9$) nanoclusters is required. Thus, the stable $\text{In}_{12}\text{N}_{12}$ unit was selected as an ideal building block [9] for designing various possible initial geometries of self-assembled $(\text{InN})_{12n}$ nanowires and nanosheets.

Table 1. Symmetry point groups (sym), average natural charges of In atoms (NC), dipole moment (Dip), isomers (iso), HOMO and LUMO gaps (E_{gap}), average InN diatomic binding energies ($E_{\text{b}}(n)$), fragmentation energies ($D(n, n-1)$), lowest frequencies (Freq), and total energies (E_{T}) of the most stable $(\text{InN})_{12n}$ ($n = 1-8$) nanosheets. The stable geometries with $\text{In}_{12}\text{N}_{12}$ connected by six-membered rings.

| Systems | Sym | Iso | NC | Dip Debye | HOMO Hartree | LUMO Hartree | Freq cm^{-1} | E_{gap} eV | ET Hartree | $E_{\text{b}}(n)$ eV | $D(n, n-1)$ eV |
|-------------------------------|----------------|-----|-------|--------------|-----------------|-----------------|--------------------------|------------------------|---------------|-------------------------|-------------------|
| $\text{In}_{12}\text{N}_{12}$ | T_{h} | a | 1.703 | 0.00 | -0.22082 | -0.13050 | 71.3 | 2.46 | -678.876339 | 4.048 | |
| $\text{In}_{24}\text{N}_{24}$ | C_1 | a | 1.745 | 0.00 | -0.21941 | -0.12626 | 35.5 | 2.53 | -1358.084415 | 4.424 | 9.03 |
| $\text{In}_{36}\text{N}_{36}$ | S_6 | a | 1.760 | 0.01 | -0.22161 | -0.13177 | 20.3 | 2.44 | -2037.291826 | 4.549 | 9.01 |
| | C_1 | b | 1.755 | 5.21 | -0.20426 | -0.13521 | 26.4 | | -2037.234748 | | |
| $\text{In}_{48}\text{N}_{48}$ | C_1 | a | 1.783 | 0.01 | -0.21476 | -0.12515 | 27.8 | 2.44 | -2716.706404 | 4.729 | 14.645 |
| | C_1 | b | 1.764 | 5.61 | -0.20392 | -0.13396 | 17.3 | | -2716.439412 | | |
| $\text{In}_{60}\text{N}_{60}$ | C_1 | a | 1.782 | 4.96 | -0.20447 | -0.13361 | 18.0 | 1.93 | -3395.863320 | 4.720 | 7.635 |
| | C_1 | b | 1.598 | 6.99 | -0.20888 | -0.13552 | 10.2 | | -3395.596897 | | |
| | C_1 | c | 1.767 | 0.01 | -0.21577 | -0.12998 | 10.9 | | -3395.595081 | | |
| | C_1 | d | 1.769 | 1.69 | -0.21508 | -0.12642 | 10.0 | | -3395.652494 | | |
| $\text{In}_{72}\text{N}_{72}$ | C_1 | a | 1.776 | 0.01 | -0.21425 | -0.12415 | 18.4 | 2.45 | -4075.341547 | 4.835 | 16.377 |
| | C_1 | b | 1.776 | 5.02 | -0.23520 | -0.12284 | 13.0 | | -4074.968946 | | |
| | C_1 | c | 1.781 | 6.22 | -0.20437 | -0.13344 | 14.3 | | -4075.029513 | | |
| | C_1 | d | 1.783 | 4.05 | -0.20435 | -0.13351 | 12.9 | | -4075.067931 | | |
| $\text{In}_{84}\text{N}_{84}$ | C_1 | a | 1.794 | 4.88 | -0.20397 | -0.13304 | 12.5 | 1.93 | -4754.498871 | 4.814 | 7.646 |
| | C_1 | b | 1.794 | 6.24 | -0.20149 | -0.13028 | 15.2 | | -4754.495491 | | |
| | C_1 | c | 1.681 | 4.54 | -0.20426 | -0.13145 | 13.2 | | -4754.455641 | | |
| | C_1 | d | 1.779 | 5.61 | -0.20761 | -0.12881 | 9.5 | | -4754.198775 | | |
| | C_1 | e | 1.776 | 7.18 | -0.20362 | -0.13557 | 9.9 | | -4754.111104 | | |
| $\text{In}_{96}\text{N}_{96}$ | C_1 | a | 1.803 | 0.04 | -0.21351 | -0.12356 | 12.0 | 2.45 | -5433.976634 | 4.889 | 16.365 |
| | C_1 | b | 1.802 | 1.91 | -0.21697 | -0.12618 | 11.4 | | -5433.936053 | | |
| | C_1 | c | 1.791 | 0.20 | -0.21141 | -0.12803 | 6.8 | | -5433.655668 | | |
| | C_1 | d | 1.795 | 0.02 | -0.20682 | -0.12777 | 10.6 | | -5433.515520 | | |
| | C_1 | e | 1.793 | 1.71 | -0.21340 | -0.12581 | 9.3 | | -5433.712151 | | |

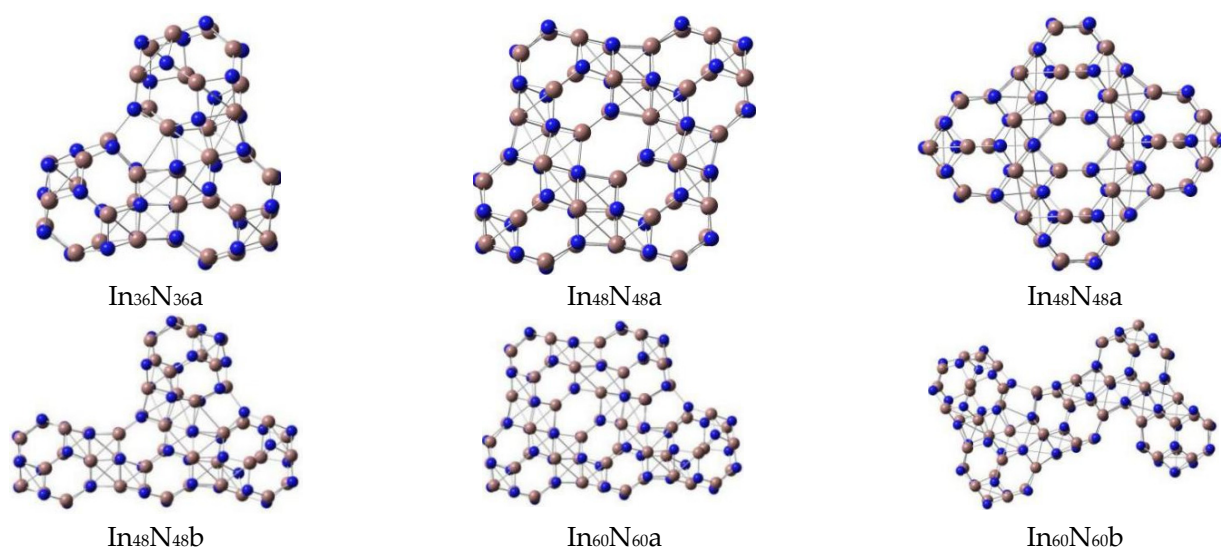


Figure 1. Cont.

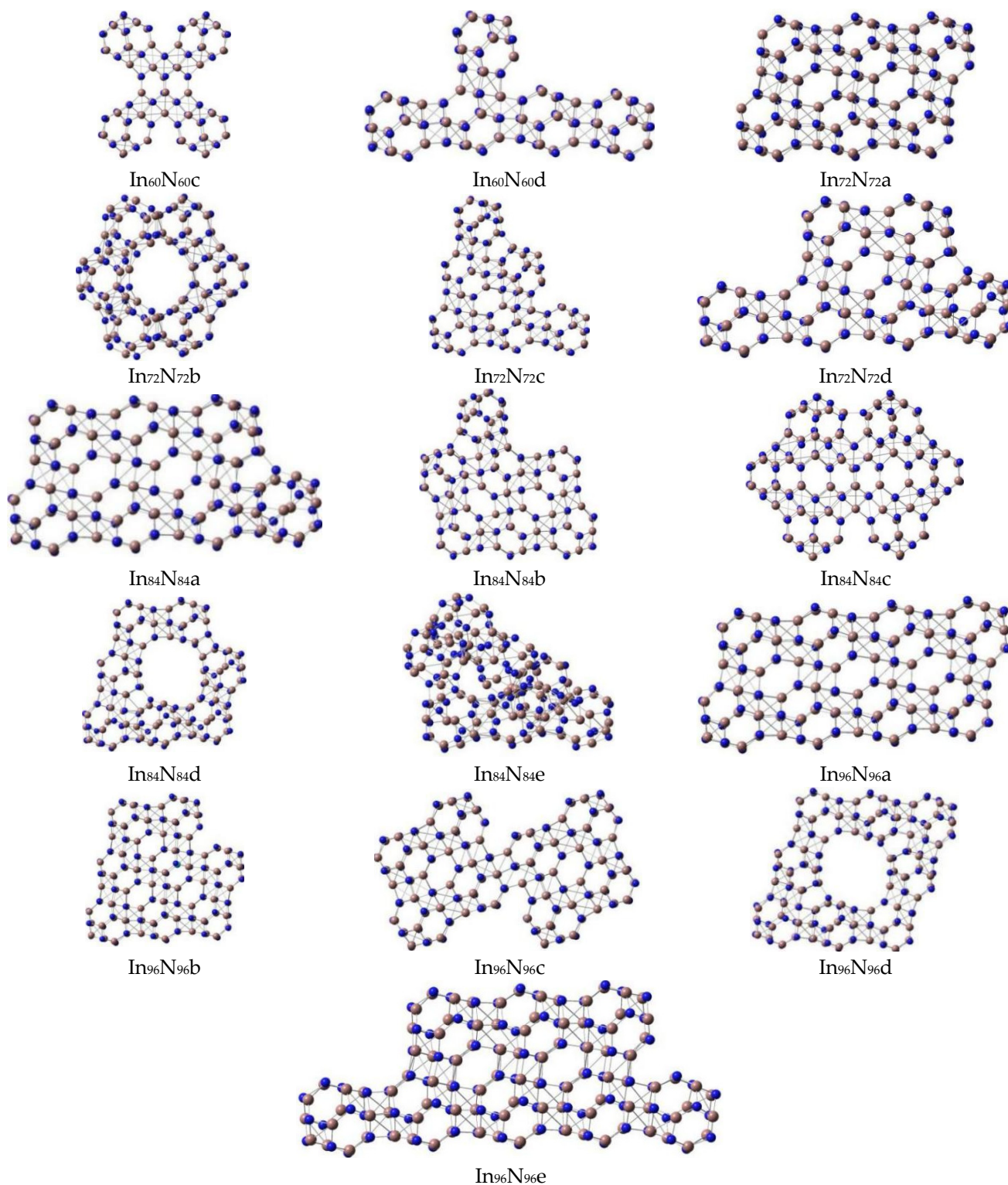


Figure 1. The stable $(\text{InN})_{12n}$ ($n = 1\text{--}8$) nanosheets with $\text{In}_{12}\text{N}_{12}$ units combined by their six-membered rings.

Table 2. Symmetry point groups (sym), average natural charges of In atoms (NC), dipole moment (Dip), isomers (Iso), HOMO and LUMO gaps (E_{gap}), average InN diatomic binding energies ($E_b(n)$), fragmentation energies ($D(n, n-1)$), lowest frequencies (Freq), and total energies (E_T) of the most stable $(\text{InN})_{12n}$ ($n = 1-9$) nanowires. The stable geometries with $\text{In}_{12}\text{N}_{12}$ connected by six-membered rings.

| Systems | Sym | Iso | NC | Dip Debye | HOMO Hartree | LUMO Hartree | Freq cm^{-1} | E_{gap} eV | E_T Hartree | $E_b(n)$ eV | $D(n, n-1)$ eV |
|---------------------------------|-------|-----|-------|--------------|-----------------|-----------------|--------------------------|------------------------|------------------|----------------|-------------------|
| $\text{In}_{12}\text{N}_{12}$ | T_h | a | 1.703 | 0.00 | -0.22082 | -0.13050 | 71.3 | 2.46 | -678.876339 | 4.048 | |
| $\text{In}_{24}\text{N}_{24}$ | C_1 | a | 1.745 | 0.00 | -0.21941 | -0.12626 | 35.5 | 2.53 | -1358.084415 | 4.424 | 9.03 |
| $\text{In}_{36}\text{N}_{36}$ | S_6 | a | 1.760 | 0.01 | -0.22161 | -0.13177 | 20.3 | 2.44 | -2037.291826 | 4.549 | 9.01 |
| $\text{In}_{48}\text{N}_{48}$ | C_1 | c | 1.767 | 0.00 | -0.21813 | -0.12329 | 12.4 | 2.59 | -2716.498627 | 4.611 | 9.01 |
| $\text{In}_{60}\text{N}_{60}$ | C_1 | e | 1.771 | 0.04 | -0.21783 | -0.12264 | 8.5 | 2.57 | -3395.706352 | 4.649 | 9.02 |
| $\text{In}_{72}\text{N}_{72}$ | C_1 | e | 1.774 | 0.01 | -0.21772 | -0.12218 | 5.2 | 2.60 | -4074.911066 | 4.673 | 8.94 |
| $\text{In}_{84}\text{N}_{84}$ | C_1 | f | 1.776 | 0.02 | -0.21755 | -0.12193 | 3.9 | 2.60 | -4754.118833 | 4.691 | 9.02 |
| $\text{In}_{96}\text{N}_{96}$ | C_1 | f | 1.778 | 0.01 | -0.21741 | -0.12181 | 2.7 | 2.60 | -5433.322507 | 4.703 | 8.91 |
| $\text{In}_{108}\text{N}_{108}$ | C_1 | a | 1.778 | 0.01 | -0.21724 | -0.12178 | 1.8 | 2.597 | -6112.528888 | 4.714 | 8.98 |

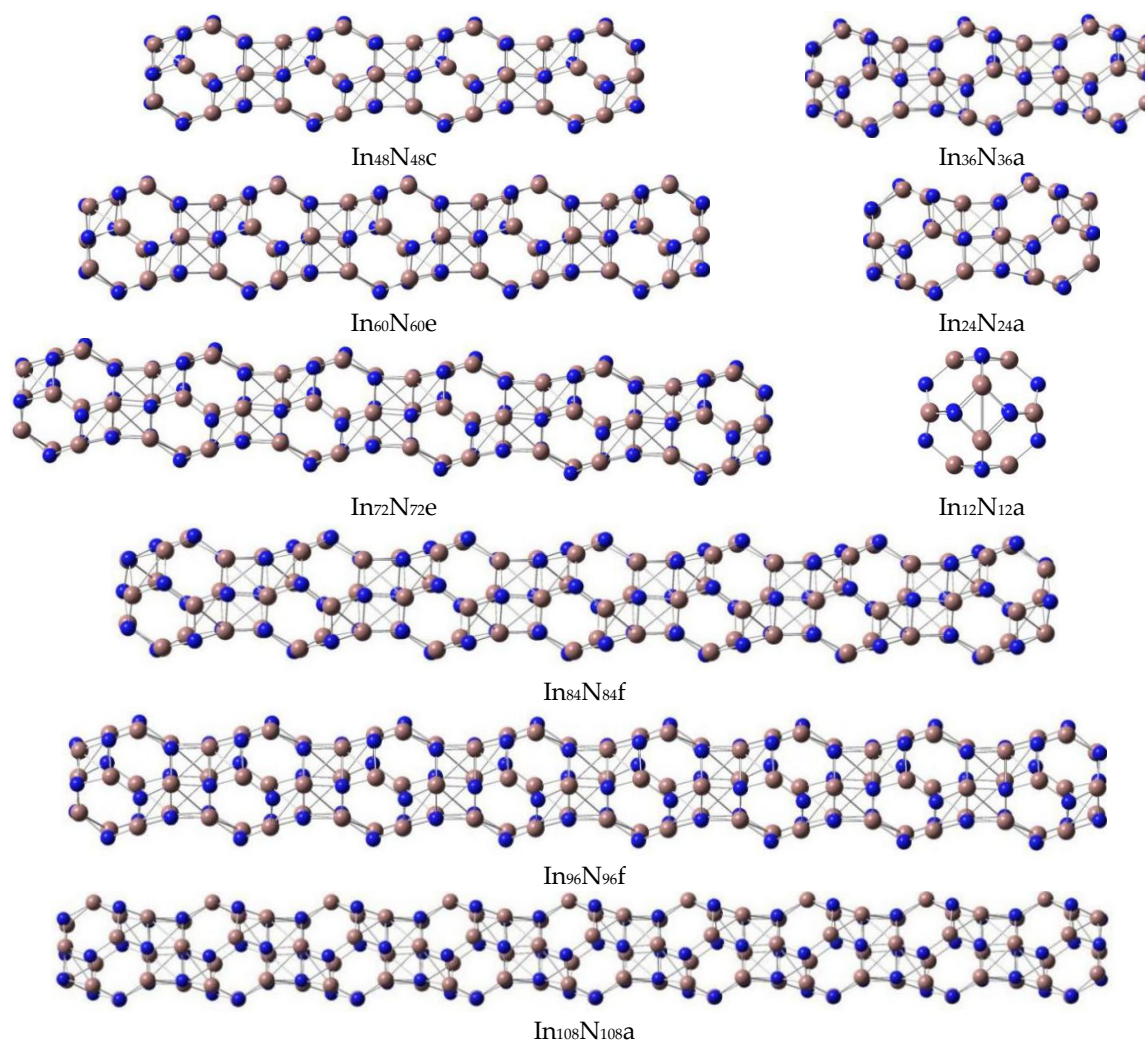


Figure 2. The stable $(\text{In}_{12}\text{N}_{12})_n$ ($n = 1-9$) nanowires connected by six-membered rings.

All possible geometries of $(\text{InN})_{12n}$ ($n = 1-9$) nanowires and $(\text{InN})_{12n}$ ($n = 1-8$) nanosheets were optimized at the PBE1PBE level with a size in the regions of 5.1~63.4 Å. The $(\text{InN})_{12n}$ ($n = 1-9$) nanoclusters (nanosheets and nanowires) were composed of many stable individual $(\text{InN})_{12}$ units (Figures 1 and 2) connected by hexagonal prisms formed

by six-membered rings in different $(\text{InN})_{12}$ units. In particular, the stable geometries of the $(\text{InN})_{12n}$ ($n = 1-9$) nanowires formed by self-assembly of a number of $(\text{InN})_{12}$ units (Figure 2) were optimized to be stable linear forms with zero dipole moments and higher point group symmetry (Table 2).

According to the calculated dipole moment of the $\text{In}_{24}\text{N}_{24}$ unit in Table 1, the optimized geometry of the $\text{In}_{24}\text{N}_{24}$ nanowire is presented as a linear structure, which was composed of two $(\text{InN})_{12}$ units. The N-In bond lengths in each $(\text{InN})_{12}$ unit of $\text{In}_{24}\text{N}_{24}$ nanowire were predicted to be 2.27 (four-membered ring) and 2.12 Å (six-membered ring). The In-N connecting distance between two $(\text{InN})_{12}$ units was 2.14 Å, and these values demonstrate that the stable geometry of each $(\text{InN})_{12}$ unit in the $\text{In}_{24}\text{N}_{24}$ nanowire was slightly changed under the interactions between two $(\text{InN})_{12}$ units after both $(\text{InN})_{12}$ units were combined. In particular, the stable $(\text{InN})_{12}$ geometry near the connecting part deviated slightly from its original individual form. However, the $(\text{InN})_{12}$ geometry, which was not involved in the connecting section, being 2.01 (or 2.00) Å for hexagons (six-member rings) and 2.09 Å for squares (four-member rings), maintained the geometrical form of its individual isolated $(\text{InN})_{12}$ unit. As far as the $\text{In}_{36}\text{N}_{36}$ isomers are concerned, two possible $\text{In}_{36}\text{N}_{36}$ isomers were considered and optimized as stable structures. The energetically favorable $\text{In}_{36}\text{N}_{36}$ geometry with a zero dipole moment was the linear form, which was lower in total energy than the triangle form and slightly deformed the higher point-group symmetry, reflecting that linear $\text{In}_{36}\text{N}_{36}$ geometry was the most stable one. The linear geometry of $\text{In}_{36}\text{N}_{36a}$ is shown in Figure 2, and its total energy was higher than that of $\text{In}_{36}\text{N}_{36b}$, which is shown in Figure 1.

A variety of possible initial geometrical forms were optimized for $\text{In}_{48}\text{N}_{48}$ geometries. The four stable $\text{In}_{48}\text{N}_{48}$ geometries are illustrated in Figures 1 and 2. For the optimized $\text{In}_{48}\text{N}_{48}$ geometries, the most stable rhombus $\text{In}_{48}\text{N}_{48a}$ geometry was selected as the ground state and its dipole moment was calculated to be 0.01 Debye. The $\text{In}_{48}\text{N}_{48b}$ was seen to be an $(\text{InN})_{12}$ cage capped on the linear $\text{In}_{36}\text{N}_{36}$ geometry. This geometry was slightly bigger in total energy than the linear $\text{In}_{48}\text{N}_{48c}$ cluster. After one $(\text{InN})_{12}$ unit was capped on the $\text{In}_{48}\text{N}_{48a}$ rhombus geometry, the newly formed nonlinear $\text{In}_{60}\text{N}_{60a}$ nanosheet was generated, which was the lowest-energy structure. The $\text{In}_{60}\text{N}_{60b}$, $\text{In}_{60}\text{N}_{60c}$, and $\text{In}_{60}\text{N}_{60d}$ isomers were yielded by inserting one $\text{In}_{12}\text{N}_{12}$ unit into the $\text{In}_{48}\text{N}_{48b}$ structure. Moreover, the total energies of these geometries were higher than those of the linear $\text{In}_{60}\text{N}_{60e}$ isomer, reflecting that the linear $\text{In}_{60}\text{N}_{60e}$ structure was more stable than those of the $\text{In}_{60}\text{N}_{60b}$, $\text{In}_{60}\text{N}_{60c}$, and $\text{In}_{60}\text{N}_{60d}$ isomers; however, it was less stable than that of the $\text{In}_{60}\text{N}_{60a}$ nanosheet.

According to the optimized stable $\text{In}_{72}\text{N}_{72}$ geometries, the newly formed rhombus $\text{In}_{72}\text{N}_{72a}$ geometry was the most stable geometry, and its dipole moment was predicted to be 0.01 Debye, which was generated from the $\text{In}_{60}\text{N}_{60a}$ nanosheets via the addition of a new $\text{In}_{12}\text{N}_{12}$ unit; moreover, this geometry deviated slightly to the higher point-group symmetry. It should be mentioned that the linear $\text{In}_{72}\text{N}_{72e}$ geometry was less stable energetically than the $\text{In}_{72}\text{N}_{72b}$, $\text{In}_{72}\text{N}_{72c}$, $\text{In}_{72}\text{N}_{72d}$, and $\text{In}_{72}\text{N}_{72e}$ geometries.

Following these procedures, $\text{In}_{84}\text{N}_{84a}$ and $\text{In}_{84}\text{N}_{84b}$ isomers, which were generated from the $\text{In}_{72}\text{N}_{72a}$ geometry, were investigated. As seen in Tables 1 and 2, it is exhibited that the calculated total energy difference between $\text{In}_{84}\text{N}_{84a}$ and $\text{In}_{84}\text{N}_{84b}$ was 0.092 eV, and the total energy of the $\text{In}_{84}\text{N}_{84b}$ geometry was slightly higher than that of $\text{In}_{84}\text{N}_{84a}$. Consequently, $\text{In}_{84}\text{N}_{84a}$ was more stable than the $\text{In}_{84}\text{N}_{84b}$ nanosheet, and the $\text{In}_{84}\text{N}_{84a}$ nanosheet was confirmed to be the most stable geometry. In particular, the $\text{In}_{84}\text{N}_{84c}$ nanosheet was obtained by combining two $\text{In}_{48}\text{N}_{48a}$ units together, and it was less stable than the $\text{In}_{84}\text{N}_{84b}$ nanosheet. The $\text{In}_{84}\text{N}_{84e}$ nanosheet, which deformed the plane-like form, was only higher in total energy than the linear $\text{In}_{84}\text{N}_{84f}$ geometry. However, the energy gap of the linear $\text{In}_{84}\text{N}_{84f}$ geometry (2.60 eV) was bigger than that (2.45 eV) of the most stable $\text{In}_{84}\text{N}_{84a}$ structure. Eventually, the distinct characteristic of the energy gap of linear geometry was increased with the size of the cluster being extended. In particular, an energy gap of an $\text{In}_{84}\text{N}_{84f}$ nanowire being 2.60 eV is in the range suitable for optoelectronic devices that emit in the visible region. The formation of semiconductor

nanowires with an energy gap in the visible region of 1.62~3.11 eV has potential applications in the fields of nanophotonics, nanoelectronics, and medicine, which are consistent with the experimental results.

All possible $\text{In}_{96}\text{N}_{96}$ isomers were considered, and six possible $\text{In}_{96}\text{N}_{96}$ nanoclusters were optimized to be stable geometries. The stable $\text{In}_{96}\text{N}_{96}\text{a}$ nanosheet was generated by capping one $\text{In}_{12}\text{N}_{12}$ unit on the $\text{In}_{84}\text{N}_{84}\text{a}$ or $\text{In}_{84}\text{N}_{84}\text{b}$ isomers. The $\text{In}_{96}\text{N}_{96}\text{a}$ nanosheet with a dipole moment of 0.04 Debye was lower in total energy by 1.104 eV than the $\text{In}_{96}\text{N}_{96}\text{b}$ nanosheet. Consequently, the $\text{In}_{96}\text{N}_{96}\text{a}$ nanosheet was more stable than the $\text{In}_{96}\text{N}_{96}\text{b}$ nanosheet; the formation of the $\text{In}_{96}\text{N}_{96}\text{c}$ nanosheet was based on the combination of two $\text{In}_{48}\text{N}_{48}$ units, and the $\text{In}_{96}\text{N}_{96}\text{c}$ nanosheet was less stable than both $\text{In}_{84}\text{N}_{84}\text{a}$ and the $\text{In}_{84}\text{N}_{84}\text{b}$ isomers. The interesting rhombus $\text{In}_{96}\text{N}_{96}\text{d}$ nanosheet yielded a big hole in the center; this stable isomer can be suitable for hosting new clusters or molecules for application in porous nanomaterials. According to the calculated results in Table 1 and Figure 1, the $\text{In}_{96}\text{N}_{96}\text{e}$ nanosheet was also obtained from the $\text{In}_{84}\text{N}_{84}\text{a}$ nanosheet, and this structure was more stable than both the $\text{In}_{96}\text{N}_{96}\text{c}$ and the $\text{In}_{96}\text{N}_{96}\text{d}$ nanosheets. Finally, the linear $\text{In}_{96}\text{N}_{96}$ geometry is mentioned, and this isomer had the same energy gap (2.60 eV) as the linear $\text{In}_{72}\text{N}_{72}$ and $\text{In}_{84}\text{N}_{84}$ isomers (Figure 2 and Table 2). In particular, the energy gap of the $\text{In}_{108}\text{N}_{108}$ nanowire was determined to be 2.59 eV, which was slightly smaller than those of the $\text{In}_{72}\text{N}_{72}$, $\text{In}_{84}\text{N}_{84}$, and $\text{In}_{96}\text{N}_{96}$ nanowires.

3.2. Relative Stabilities

The relative stabilities of $(\text{InN})_{12n}$ nanoclusters consisting of different In and N atoms were investigated based on the average InN diatomic binding energies ($E_b(n)$) as well as the calculated fragmentation energies ($D(n, n-1)$), which are defined as

$$E_b(n) = \frac{12n * E_T(\text{InN}) - E_T[(\text{InN})_{12n}]}{12n} \quad (1)$$

$$D(n, n-1) = E_T[(\text{InN})_{12(n-1)}] + E_T(\text{InN})_{12} - E_T[(\text{InN})_{12n}] \quad (2)$$

where $E_T[(\text{InN})_{12n}]$, $E_T(\text{InN})$, and $E_T[(\text{InN})_{12(n-1)}]$ are the calculated total energies of the respective $(\text{InN})_{12n}$ and $(\text{InN})_{12(n-1)}$ nanoclusters, together with the InN dimer, with zero-point vibration energies being taken into accounts. The total energy of the InN diatom was predicted to be -56.424257 Hartree.

Although the $(\text{InN})_{12n}$ nanowires were relative weak in stability compared to the $(\text{InN})_{12n}$ nanosheets, the promising potential applicability of $(\text{InN})_{12n}$ nanowires is very unique because a newly type of semiconductor $(\text{InN})_{12n}$ nanowire in a radius within the region of a few tens of nanometers is considered to be the ideal candidate for further developing optoelectronic and electronic nanodevices. Thus, the relative stabilities of $(\text{InN})_{12n}$ nanowires are considered and discussed in detail in this study due to their unique semiconductor properties. According to our calculated relative stabilities of $(\text{InN})_{12n}$ nanowires connected by six-membered rings, the average InN diatomic binding energy ($E_b(n)$) of $(\text{InN})_{12n}$ nanowires increased continually to the maximum value of 4.714 eV when the size of $(\text{InN})_{12n}$ nanowires varied from $n = 1$ to $n = 9$. In order to demonstrate the reliability of the averaged InN diatomic binding energies of $(\text{InN})_{12n}$ nanowires, the fragmentation energies ($D(n, n-1)$) of $(\text{InN})_{12n}$ nanowires were also taken into accounts. As seen from the curves of the fragmentation energies as a function of size (Figure 3 for $(\text{InN})_{12n}$ nanowires), the apparent tendency for $(\text{InN})_{12n}$ nanowires was that their fragmentation energies decreased as the size of $(\text{InN})_{12n}$ nanowires varied from $n = 1$ to $n = 9$ (Figure 3). In general, the calculated values of the fragmentation energies for the $(\text{InN})_{12n}$ nanowires exhibited an alternating even-odd oscillation, with the even-numbered $(\text{InN})_{12n}$ nanowire (n is even) being smaller in fragmentation energy than its odd-numbered neighboring $(\text{InN})_{12n}$ nanowires (n is odd), reflecting that the odd-numbered semiconductor $(\text{InN})_{12n}$ nanowires had stronger stability than their neighboring even-numbered semiconductor $(\text{InN})_{12n}$ nanowires.

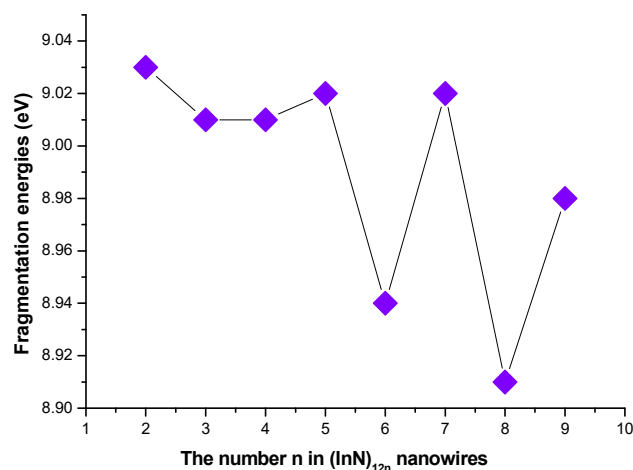


Figure 3. The calculated fragmentation energies of $(\text{InN})_{12n}$ nanowires.

The average InN diatomic binding energies of the stable $(\text{InN})_{12n}$ nanoclusters (including nanowires and nanosheets) are listed in Tables 1 and 2 and shown in Figure 4. Based on the calculated average InN diatomic binding energy for $(\text{InN})_{12n}$ nanoclusters, the magic numbers of stabilities for $(\text{InN})_{12n}$ nanoclusters were assigned at $n = 2, 4, 6,$ and 8 , reflecting that the even-membered semiconductor $(\text{InN})_{12n}$ nanoclusters (n is even) were apparently more stable compared with their neighboring odd-numbered n in $(\text{InN})_{12n}$ ($n > 2$) units.

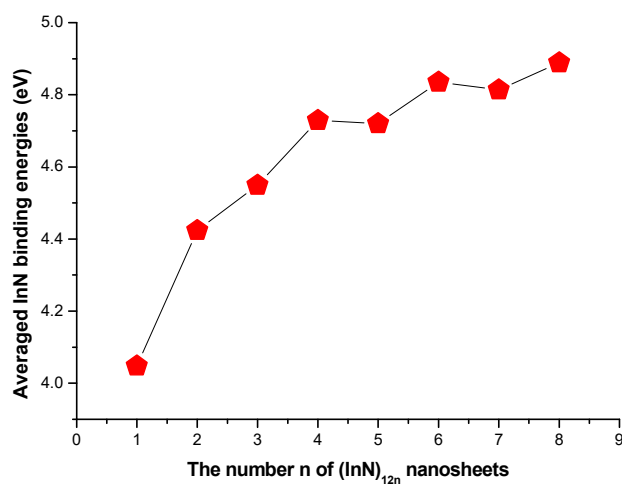


Figure 4. The calculated average InN diatomic binding energies of $(\text{InN})_{12n}$ nanosheets.

Based on the calculated $D(n, n-1)$ of $(\text{InN})_{12n}$ nanoclusters (nanowires and nanosheets) shown in the curve in Figure 5, the calculated fragmentation energies for $(\text{InN})_{12n}$ nanoclusters had the same tendency as those of $(\text{InN})_{12n}$ nanowires mentioned above, with the calculated values of fragmentation energies for $(\text{InN})_{12n}$ nanoclusters generally showing an appealing even–odd oscillation. On the contrary, the even-numbered semiconductor $(\text{InN})_{12n}$ nanoclusters (where n is even) had higher fragmentation energy than the odd-numbered ones, suggesting that the even-numbered nano-size $(\text{InN})_{12n}$ (where n is even) clusters had stronger stability compared with their odd-numbered $(\text{InN})_{12n}$ neighbors. The remarkable peaks were $n = 4, 6,$ and 8 . Interestingly, the $\text{In}_{72}\text{N}_{72}$ and $\text{In}_{96}\text{N}_{96}$ nanosheets, with $n = 6$ and 8 , respectively, were composed of individual $(\text{InN})_{48}$ ($n = 4$) units, indicating that $\text{In}_{72}\text{N}_{72}$ and $\text{In}_{96}\text{N}_{96}$ nanosheets were generated by the primarily newly formed $\text{In}_{48}\text{N}_{48}$ nanosheets; thus, one can infer that even-numbered $(\text{InN})_{12n}$ can be detected more easily with mass spectroscopy experimental measurements with remarkably large abundances than the neighboring odd-numbered $(\text{InN})_{12n}$ ones. More importantly, the $(\text{InN})_{12n}$ nanosheet with $n = 4$ was assigned as a newly formed self-assembled building

block for new film nanosheets. Eventually, the $(\text{InN})_{48a}$ nanosheet was selected as the newly formed building block for self-assembled $(\text{InN})_{12n}$ semiconductor film nanosheets (or nanomembranes), which have an important application in microelectronic and optoelectronic nanodevices. They can form the magnetic nanomembrane after magnetic metal atoms or ions are inserted in a suitable hole in $(\text{InN})_{12n}$ nanosheets.

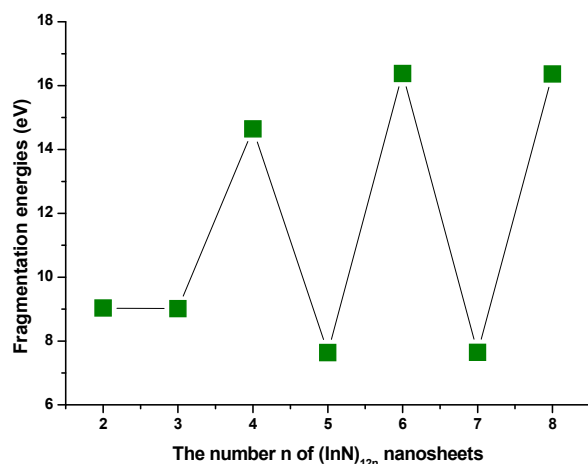


Figure 5. The calculated fragmentation energies of $(\text{InN})_{12n}$ nanosheets.

3.3. HOMO-LUMO Gaps

The electronic properties of self-assembled $(\text{InN})_{12n}$ nanoclusters (including both nanowires and nanosheets) associated with the calculated energy gap values between HOMO (the highest occupied molecular orbital level) and LUMO (the lowest unoccupied molecular orbital level) were investigated. The predicted HOMO-LUMO energy gaps of $(\text{InN})_{12n}$ nanoclusters are summarized in Tables 1 and 2 and shown in Figure 6.

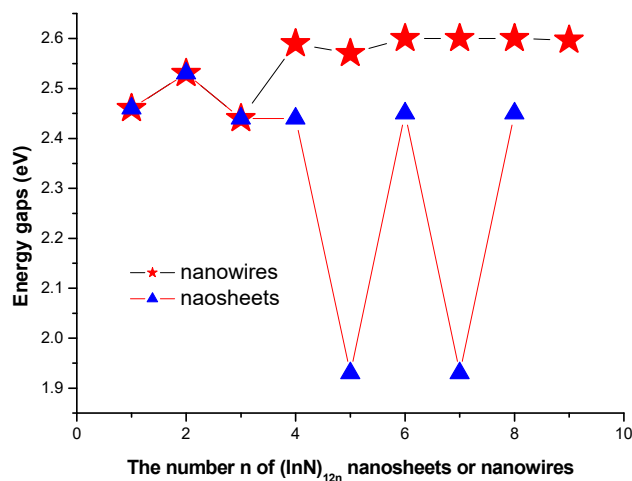


Figure 6. Energy gaps of $(\text{InN})_{12n}$ nanowires or nanosheets as a function of the size of the nanowires or nanosheets, respectively.

Based on a theoretical point of view, the advantages of $(\text{InN})_{12n}$ nanowires are that they are ideal models for further investigation and development of optoelectronic and electronic nanodevices. In order to reveal the geometrical and electronic properties of $(\text{InN})_{12n}$ nanowires, DFT studies were performed. According to the calculated energy gaps of $(\text{InN})_{12n}$ nanowires listed in Table 1 and shown in Figure 6, it is obvious that the obtained energy gap values of $(\text{InN})_{12n}$ nanowires were oscillatory, increasing at the small size and finally reaching a maximum of 2.60 eV at the large size region of $n = 9$. Obviously, the calculated energy gap values of $(\text{InN})_{12n}$ nanowires connected by six-membered rings

varied slightly when the size of $(\text{InN})_{12n}$ nanowires changed from $n = 1$ to $n = 9$. This varying tendency of the energy gaps in semiconductor $(\text{InN})_{12n}$ ($n = 1-9$) nanowires is actually consistent with that of inner hollow InN nanoclusters [9]. Therefore, the $(\text{InN})_{12n}$ nanowires almost maintained the energy gap properties of an individual $\text{In}_{12}\text{N}_{12}$ unit; consequently, the variations in the energy gaps in $(\text{InN})_{12n}$ ($n = 1-9$) nanowires were indeed small when the size n of $(\text{InN})_{12n}$ nanowires varied from $n = 1$ to $n = 9$. The varying tendency of the energy gaps in $(\text{InN})_{12n}$ nanowires may have directly led to a quantum size effect. Moreover, the slight variations in the energy gaps for the semiconductor $(\text{InN})_{12n}$ ($n = 1-9$) nanowires revealed that the $(\text{InN})_{12n}$ nanowires possessed the analogue characteristics and properties of individual $(\text{InN})_{12}$ units [9]. The calculated energy gaps of the semiconductor $(\text{InN})_{12n}$ nanowires at the approved 2.44~2.60 eV regions were obviously within the visible light region, indicating that the size of the nanowires generated small influences on their energy gaps and reflecting that this kind of $(\text{InN})_{12n}$ nanowire can give rise to the widespread applications in the fields of nanophotonics and nanoelectronics. Moreover, the unique HOMO-LUMO properties of semiconductor $(\text{InN})_{12n}$ nanowires are receiving extremely noteworthy attention and promoted research, resulting in the opportunity for the widespread development of nanodevices and surface sciences.

The energy gap values for $(\text{InN})_{12n}$ nanoclusters (nanowires and nanoclusters) were calculated and are shown in Figure 6. According to the calculated energy gap values of $(\text{InN})_{12n}$ nanoclusters, it is exhibited that the obtained energy gaps of $(\text{InN})_{12n}$ nanosheets within the range of 1.93~2.53 eV depended on the varied size of the nanosheets, reflecting that cluster-assembled $(\text{InN})_{12n}$ nanosheets are good semiconductor optoelectronic or energy nanomaterials and give rise to attractive optical and electrooptical properties. The variation in the HOMO-LUMO gaps of $(\text{InN})_{12n}$ nanowires was smaller than that of $(\text{InN})_{12n}$ nanosheets as their size was extended. The HOMO-LUMO gaps (energy gaps) of even-numbered $(\text{InN})_{12n}$ nanosheets were bigger than those of the neighboring odd-numbered $(\text{InN})_{12n}$ nanosheets. The maximum value of the energy gap (2.53 eV) was assigned as $n = 2$, and the corresponding $(\text{InN})_{24}$ nanosheet had the strongest chemical stability. The minimum values of energy gaps (1.93 eV) were assigned as $n = 5$ and $n = 7$, and the $(\text{InN})_{60}$ and $(\text{InN})_{72}$ nanosheets had the weakest chemical stability and the strongest chemical activity, respectively. Moreover, the relative stabilities of $(\text{InN})_{12n}$ nanosheets with $n = 5$ and $n = 7$ were weakened compared to the neighboring $(\text{InN})_{12n}$ nanosheets in that their nanostructures could be elucidated as smaller energy gaps with stronger chemical activity, reflecting that the surfaces of the $(\text{InN})_{12n}$ nanosheets with $n = 5$ and $n = 7$ could react easily with a new $(\text{InN})_{12}$ unit, and stable $(\text{InN})_{12(n+1)}$ nanosheets were achieved. This process is a cluster-cluster chemical reaction. In fact, the growth and formation of new nanoclusters (nanosheets and nanowires) are deeply involved in the catalytic process; in the other words, the cluster-assembled nanoclusters (nanosheets and nanowires) on the surface of film actually undergo chemical processes. Thus, $(\text{InN})_{12n}$ with $n = 4, 6$, and 8 had remarkably larger abundances in experimental measurements due to their chemical stabilities. This finding is consistent with our discussions on relative stabilities in this manuscript. Moreover, the energy gaps of $(\text{InN})_{12n}$ nanosheets are more favorable for optoelectronic applications than the reported experimental and theoretical findings [14–17]. These dimensionally uniform self-assembled $(\text{InN})_{12n}$ nanosheets or nanowires may surmount the difficulties of lower efficiency, lower power, and lower quantum effect in monolayer $(\text{InN})_{12n}$ nanosheets.

3.4. Natural Charge Population Analysis

The average natural atomic charge populations of indium atoms in the $(\text{InN})_{12n}$ nanowires and nanosheets were obtained at the PBE1PBE level. The calculated average natural atomic charge populations for indium atoms are plotted in Figure 7. Based on the average natural atomic charge populations of indium atoms for all sizes of $(\text{InN})_{12n}$ nanoclusters (including nanowires and nanosheets) tabulated in Tables 1 and 2, it is evident that the charges in the self-assembled $(\text{InN})_{12n}$ nanoclusters were transferred from the indium atoms to their neighboring nitrogen atoms, reflecting that the surface In atom in

(InN)_{12n} nanoclusters behaved like a Lewis acid site, whereas the electronegative nitrogen atoms behaved as a Lewis base site, and that they are appropriate sites for possible carbonylation by a CO₂ molecule. The In and N atoms in the (InN)_{12n} nanoclusters were chemically bonded with oxygen and carbon atoms, respectively, in CO₂. Thus, (InN)_{12n} nanoclusters are suitable for decomposing a CO₂ molecule. As can be seen from Tables 1 and 2 and Figure 7, there was an increasing trend of the average natural atomic charge population of indium atoms in (InN)_{12n} nanoclusters with the increasing size of (InN)_{12n} nanoclusters; the electronic charges in the N atoms originated from the neighboring In atoms. As far as the average natural atomic charge populations of indium atoms in (InN)_{12n} nanowires are concerned, the maximum average natural atomic charge population values of In atoms of 1.774 and 1.778 corresponded to two remarkable peaks of (InN)_{12n} nanowires with n = 6 and n = 8, respectively, at the curve in Figure 7. However, the local maximum average natural atomic charge population values for indium atoms in (InN)_{12n} nanosheets of 1.783 and 1.803 corresponded to two remarkable peaks with n = 4 and n = 8, respectively, in Figure 7. Electrostatic interactions among all In and N atoms in (InN)_{12n} nanoclusters resulting from charge transfers increased when the size of (InN)_{12n} nanoclusters increased; therefore, the electrostatic interaction enhanced the stabilities of (InN)_{12n} nanoclusters. Furthermore, the ionic bonding formed between the In and N atoms in (InN)_{12n} nanowires or nanosheets eventually enhanced the stabilities of (InN)_{12n} nanowires or nanosheets.

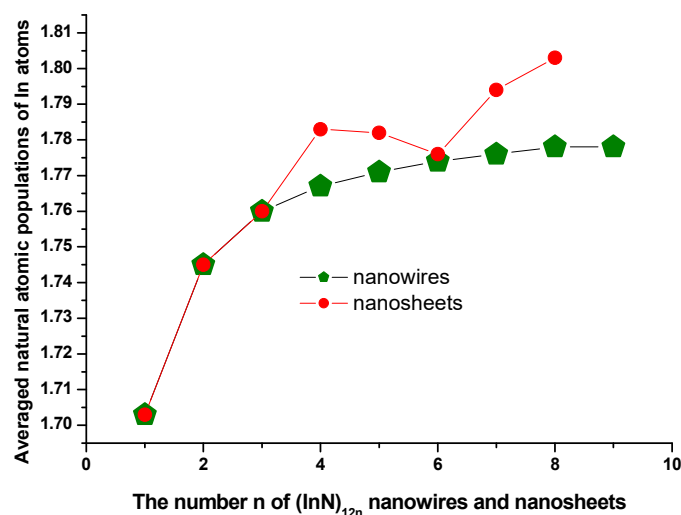


Figure 7. The average natural atomic populations of In atoms in (InN)_{12n} nanosheets or nanowires.

4. Conclusions

As for the (InN)_{12n} nanoclusters consisting of numerous In₁₂N₁₂ units that were connected by six-membered rings, a series of (InN)_{12n} nanowires or nanosheets was taken into account and their molecular structures and properties were elucidated and investigated at the PBE1PBE level. According to the calculated average InN diatomic binding energy and fragmentation energy, the relative stabilities of (InN)_{12n} nanoclusters (nanowires and nanosheets) were studied, exhibiting that the even-numbered (InN)_{12n} nanoclusters were obviously stronger in stability than their odd-numbered (InN)_{12n} neighbors. The remarkable peaks were shown at n = 4, 6, and 8. Interestingly, the most stable In₇₂N₇₂ and In₉₆N₉₆ nanosheets consisted of (InN)₄₈ nanosheets (n = 4); consequently, the (InN)₄₈ nanosheet was confirmed to be a newly formed elemental building unit for cluster-assembled nanoscale film materials. With the nanowire size increasing from n = 1 to n = 9, a number of changes in the energy gaps of the (InN)_{12n} nanowires were noted. Interestingly, the HOMO-LUMO gaps of (InN)_{12n} nanowires at the region of 2.44~2.60 eV were within the visible light region. Furthermore, the slight variation in HOMO-LUMO gaps for (InN)_{12n} nanowires reflect that (InN)_{12n} nanowires maintained their property of an individual (InN)₁₂ unit and reveal an important implication for the development of nanodevice prototypes. In summary, the

energy gaps for (InN)_{12n} nanosheets and nanowires were calculated, and the gaps of even-numbered (InN)_{12n} nanoclusters were bigger compared with those of their odd-numbered (InN)_{12n} neighbors. In addition, the obtained averaged natural atomic populations of In atoms in (InN)_{12n} nanowires or nanosheets exhibited that charge transfers, together with ionic bonding, generally increased when the size of (InN)_{12n} nanoclusters increased, and ionic bonding in (InN)_{12n} nanoclusters existed with covalent bonding. The obtained charge transfers in (InN)_{12n} nanoclusters reflect that the In atoms of (InN)_{12n} nanoclusters behaved like a Lewis acid site, whereas the electronegative N atoms acted like a Lewis base site, and they can be appropriate sites for possible carbonylation of CO₂ molecules.

Author Contributions: Conceptualization, R.Z.; methodology, R.Z., H.Z. and F.L.; software, R.Z.; validation, R.Z.; formal analysis, R.Z.; investigation, R.Z. and J.-G.H.; resources, R.Z.; data curation, R.Z. and R.C.; writing—original draft preparation, R.Z.; writing—review and editing, J.-G.H.; visualization, R.Z. and R.C.; supervision, J.-G.H.; project administration, R.Z. and J.-G.H.; funding acquisition, R.Z. All authors have read and agreed to the published version of the manuscript.

Funding: This research received no external funding.

Institutional Review Board Statement: Not applicable.

Informed Consent Statement: Not applicable.

Data Availability Statement: The data available are published the Tables of this article.

Acknowledgments: All computations were performed in the Supercomputing Center of the University of Science and Technology of China.

Conflicts of Interest: The authors declare no conflict of interest.

References

1. Jimenez-Izal, E.; Ugalde, J.M.; Matxain, J.M. *Nanocluster-Assembled Materials, Computational Modeling of Inorganic Nanomaterials*; Taylor & Francis Group, LLC: New York, NY, USA, 2016.
2. Gu, Y.B.; Xu, N.X.; Lin, M.H.; Tan, K. Structures, stabilities and properties of hollow (Al₂O₃)_n clusters (n = 10, 12, 16, 18, 24 and 33): Studied with density functional theory. *Comput. Theor. Chem.* **2015**, *1063*, 29–34.
3. Yeganeh, M.; Kafi, F.; Boochani, A. Thermoelectric properties of InN graphene-like nanosheet: A first principle study. *Micro. Nanostruct.* **2020**, *138*, 106367.
4. Castillo, R.M.d.; Salcedo, E.; Martínez, A.; Ramos, E.; Sansores, L.E. Electronic Peculiarities of a Self-Assembled M₁₂L₂₄ Nanoball (M = Pd²⁺, Cr, or Mo). *Molecules* **2019**, *24*, 771. [[CrossRef](#)] [[PubMed](#)]
5. Orek, C.; Keser, S.; Kaygili, O.; Zuchowski, P.; Bulut, N. Structures and optical properties of zinc oxide nanoclusters: A combined experimental and theoretical approach. *J. Mol. Model.* **2023**, *29*, 227.
6. Duan, X.; Huang, Y.; Cui, Y.; Wang, J.; Lieber, C.M. Indium phosphide nanowires as building blocks for nanoscale electronic and optoelectronic devices. *Nature* **2001**, *409*, 66–69. [[CrossRef](#)]
7. Zhao, R.N.; Chen, R.; Li, Q.; Duan, Y.H. Geometries, stabilities and electronic properties of photo sensitized (CdS)_{2n} (n = 5–27) nanoclusters. *J. Alloy Compd.* **2018**, *762*, 754–762.
8. Zhao, R.N.; Chen, R.; Han, J.G. Geometrical and electronic properties of the plane-like selfassembled structured (In₁₂N₁₂)_n (n = 1–9) nanomaterials based on In₁₂N₁₂ cages connecting with four-membered rings. *Micropor. Mesopor. Mat.* **2021**, *318*, 111041.
9. Zhao, R.N.; Han, J.G.; Duan, Y.H. A density functional prediction of geometries and stabilities and electronic properties of nanosize cagelike (InN)_{2n} (n = 6–27, 45, 54) semiconductor material. *Adv. Theor. Simul.* **2018**, *1*, 1800001. [[CrossRef](#)]
10. Inushima, T. Electronic structure of superconducting InN. *Sci. Technol. Adv. Mater.* **2006**, *7*, S112–S116.
11. Zhang, Q.F.; Wang, L.S.; Zheng, H.F.; Su, A.M.; Liu, X.; Xie, X.J.; Chen, Y.Z.; Peng, D.L. Effect of in situ low-temperature annealing on anomalous Hall effect in Co nanocluster-assembled granular film. *J. Alloy Compd.* **2018**, *748*, 922–928.
12. Zhao, M.; Xia, Y.; Liu, X.; Tan, Z.; Huang, B.; Song, C.; Mei, L. First-Principles Calculations of AlN Nanowires and Nanotubes: Atomic Structures, Energetics, and Surface State. *J. Phys. Chem. B* **2006**, *110*, 8764–8768. [[CrossRef](#)] [[PubMed](#)]
13. Romero, C.P.; Volodin, A.; Vece, M.D.; Paddubrouskaya, H.; Wang, H.; Vantomme, A.; Haesendonck, C.V.; Lievens, P. Passivation of cobalt nanocluster assembled thin films with hydrogen. *Thin Solid Film.* **2012**, *520*, 5584–5588. [[CrossRef](#)]
14. Farzan, M.; Elahi, S.M.; Salehi, H.; Abolhassani, M.R. An investigation of electronic and optical properties of InN nanosheet by first principle study. *Opt. Commun.* **2017**, *395*, 293. [[CrossRef](#)]
15. Podlipskas, Z.; Jurkevicius, J.; Kadys, A.; Kolenda, M.; Kovalevskij, V.; Dobrovolskas, D.; Aleksiejunas, R.; Tamulaitis, G. Extreme radiation resistance in InN. *J. Alloy Compd.* **2019**, *789*, 48–55. [[CrossRef](#)]
16. Nagai, K.; Akiyama, T.; Nakamura, K.; Ito, T. A Simple Approach to Growth Mode of InN and InGaN Thin Films on GaN(0001) Substrate. *ECS Trans.* **2020**, *98*, 155–164. [[CrossRef](#)]

17. An, Y.; He, Y.; Wei, H.; Liu, S.; Li, M.; Song, Y.; Qiu, P.; Rehman, A.; Zheng, X.; Peng, M. Metallic indium segregation control of InN thin films grown on Si(100) by plasma-enhanced atomic layer deposition. *Results Phys.* **2019**, *12*, 804–809. [[CrossRef](#)]
18. Ma, S.; He, C.; Sun, L.Z.; Lin, H.; Li, Y.; Zhang, K.W. Stability of two-dimensional PN monolayer sheets and their electronic properties. *Phys. Chem. Chem. Phys.* **2015**, *17*, 32009–32015. [[CrossRef](#)]
19. Dong, L.H.; Liu, Y.; Zhuo, Y.J.; Chu, Y.; Wang, Y.P. Effect of alien cations on the growth mode and self-assemble fashion of ZnO nanostructures. *J. Alloy Compd.* **2010**, *509*, 2021–2030. [[CrossRef](#)]
20. Wu, X.; Li, K.; Wang, H. Facile synthesis of ZnS nanostructured spheres and their photocatalytic properties. *J. Alloy Compd.* **2009**, *487*, 537–544. [[CrossRef](#)]
21. Zhang, Z.R.; Chai, C.; Song, Y.; Kong, L.; Yang, Y. A DFT study on physical properties of III-V compounds (AlN, GaN, AlP, and GaP) in the P3(1)21 phase. *Mater. Res. Express* **2021**, *8*, 025908. [[CrossRef](#)]
22. Ernzerhof, M.; Scuseria, G.E. Assessment of the Perdew—Burke—Ernzerhof exchange–correlation functional. *J. Chem. Phys.* **1999**, *110*, 5029–5036.
23. Frisch, M.J.; Trucks, G.W.; Schlegel, H.B.; Scuseria, G.E.; Robb, M.A.; Cheeseman, J.R.; Scalmani, G.; Barone, V.; Mennucci, B.; Petersson, G.A.; et al. *Gaussian09*; Gaussian, Inc.: Wallingford, CT, USA, 2009.
24. Adamo, C.; Barone, V. Toward Reliable Density Functional Methods without Adjustable Parameters: The PBE0 Model. *J. Chem. Phys.* **1999**, *110*, 6158–6170. [[CrossRef](#)]
25. Lin, L.H.; Yang, J.C.; Ning, H.M.; Hao, D.S.; Fan, H.W. Silicon–sodium binary clusters Si_nNa ($n < 10$) and their anions: Structures, thermochemistry, and electron affinities. *Theochem* **2008**, *851*, 197–206.
26. Foster, E.; Wong, B.M. Nonempirically Tuned Range-Separated DFT Accurately Predicts Both Fundamental and Excitation Gaps in DNA and RNA Nucleobases. *J. Chem. Theory Comput.* **2012**, *8*, 2682–2687. [[CrossRef](#)]
27. Wong, B.M.; Hsieh, T.H. Optoelectronic and Excitonic Properties of Oligoacenes: Substantial Improvements from Range-Separated Time-Dependent Density Functional Theory. *J. Chem. Theory Comput.* **2010**, *6*, 3704–3712. [[CrossRef](#)]
28. Chang, C.; Lin, Y.; Niu, J.; Lour, W.; Tsai, J.; Liu, W. High-Performance AlGaIn/GaN Enhancement-Mode High Electron Mobility Transistor by Two-Step Gate Recess and Electroless-Plating Approaches. *Sci. Adv. Mater.* **2021**, *13*, 30–35. [[CrossRef](#)]

Disclaimer/Publisher’s Note: The statements, opinions and data contained in all publications are solely those of the individual author(s) and contributor(s) and not of MDPI and/or the editor(s). MDPI and/or the editor(s) disclaim responsibility for any injury to people or property resulting from any ideas, methods, instructions or products referred to in the content.